

Aging Resistance and Photocatalytic Activity of a Wood Surface Coated with a Zr⁴⁺-doped SiO₂/TiO₂ Film

Zhigao Liu,^{a,b} Luning Xuan,^b and Yunlin Fu^{b,*}

A Zr⁴⁺-doped SiO₂/TiO₂ composite film (Zr⁴⁺-doped STCF) was prepared on a wood surface *via* a sol-gel method to improve its photocatalytic activity and aging resistance. The physicochemical characteristics of the composite film were analyzed by scanning electron microscopy (SEM), Fourier transform infrared spectroscopy (FTIR), X-ray diffraction (XRD), X-ray photoelectron spectroscopy (XPS), and low-temperature N₂ sorption methods. The photocatalytic degradation of methyl orange and its aging resistance under ultraviolet light were tested. The results showed that the composite film had an anatase TiO₂ crystal form, and the addition of Zr⁴⁺ to the composite film noticeably improved photocatalytic activity and aging resistance. The highest degradation percentage occurred at 0.5 wt% Zr⁴⁺ (59.2%) when the Zr⁴⁺ ion doping amount was 2.5 wt%, and the aging resistance of the composite film also peaked under these conditions. The wood surface coated with Zr⁴⁺-doped STCF exhibited strong aging resistance and photocatalytic activity, which protected the surface from discoloration and decomposition. As it degraded organic pollutants, the modified wood surface had a good self-cleaning function.

Keywords: Wood surface; Sol-gel method; Zr⁴⁺-doped SiO₂/TiO₂ composite film; Photocatalytic activity; Aging resistance

Contact information: a: College of Environmental Resources and Materials, Guangxi University, Nanning, 530004, China; b: College of Forestry, Guangxi University, Nanning, 530004, China;

* Corresponding author: fylin@126.com

INTRODUCTION

Among steel, cement, wood, and plastic, wood is the only renewable material, and it is widely used in homes, construction, and other fields due to its appearance, ecofriendly characteristics, and high strength-to-weight ratio (Yuan *et al.* 2018). However, in actual use, wood surfaces are easily disturbed by external factors and changes in physical and chemical properties, such as poor resistance to photochromism. The surface of exterior wood fades easily after illumination, which impacts its dimensional stability. The main component of lignin absorbs ultraviolet rays, which leads to the degradation of free radicals (Aloui *et al.* 2007; Yuan *et al.* 2018) and causes defects, such as deformation and cracking. The adhesion of colored pollutants to wood surfaces also changes the color and the chemical structure of the wood surface, which causes adverse effects (Rosu *et al.* 2010). Thus, these defects can seriously impact the use of wood despite its many excellent properties. Therefore, wood must be modified to improve its surface properties and make the surface hydrophobic.

The surface modification of wood can be divided into physical, chemical (organic and inorganic modification), and other methods. Physical modification, such as heat treatment, reduces the expansion value and surface roughness of Turkish eucalyptus (Korkut *et al.* 2008).

Organic polymers have been used previously in the wood coating industry, and they have a large molecular weight. Under certain conditions, cross-linking polymerization occurs *via* copolymerization to form a complex network structure that can be firmly attached to the surface of wood and result in a film. The adhesion is good, and the film formation method is simple and easy. The protective layer offers UV resistance, waterproofing, high strength, wear resistance, and decoration (Wang *et al.* 2013).

Mahendran *et al.* (2011) synthesized an acrylic acid linseed oil treatment. Acrylic acid acts as a ring-opening agent for the cycloalkyl group of the epoxy linseed oil, and it was cured with UV light on the surface of the wood to obtain better gloss. The cross-linking copolymerization of acrylic linseed oil offers scratch resistance and adhesion to the substrate. Wright *et al.* (2006) added polymer whey protein (PWP) and 0.3% antibacterial agent to wood polyurethane coating, which significantly improved the antibacterial properties of the wood and reduced the amount of antibacterial agents needed.

New technologies for wood modification include sol-gel methods to prepare magnetic microencapsulated phase change energy storage composite wood (Qian *et al.* 2019) and energy-saving dielectric barrier discharge (DBD) plasma systems applied to the surface of wood as a hydrophobic coating (Chen *et al.* 2018). The volume expansion coefficient of wood has also been studied *via* the time-dependent zeta potential of the wood surface (Muff *et al.* 2018). Guo *et al.* (2018) used photon curing to construct a copper nano-coating on the wood surface, in which the layer realizes the electrical conductivity of the wood. These wood surface methods improve the wood's surface function.

Inorganic improved wood is better than organic matter for wood surface improvement. A sol-gel method can treat the surface of the wood with inorganic materials, such as SiO₂ and TiO₂. This improves the mechanical strength, thermal stability, performance, hardness, dimensional stability, flame retardancy, photodegradability, and corrosion resistance of wood. Hubert *et al.* (2010) prepared a TiO₂ wood composite *via* a vacuum impregnation sol-gel method. This reduced the water adsorption saturation value of the wood, delayed the burning of the wood matrix, and enhanced the dimensional stability of the wood. Mahltig *et al.* (2010) used tetraethoxysilane as a precursor to hydrolysis and polycondensation under acidic conditions to form SiO₂ nanosol. This substance was coated on the surface of heat-treated wood to improve the hydrophobicity and weather resistance of the wood surface. Mahr *et al.* (2013) used the sol-gel method to study the copper ion leaching efficiency of TiO₂ and SiO₂ precursors and found that the gel layer formed on the surface and inside of the wood played a hydrophobic role. The material surface has a self-cleaning function *via* reasonable surface modification treatment.

The technology for preparing photocatalysts by doping inorganic materials with metal ions is well developed, but there have been few reports on their application on wood surfaces. In recent work, a Fe³⁺-doped SiO₂/TiO₂ film that had been coated on the surface of wood was successfully prepared, and the modified wood exhibited strong hydrophobicity and photocatalytic activity (Xuan *et al.* 2018). However, the composite film doped with various irons may bring different performance changes on the wood surface. In this study, sol-gel technology was used to load silicon-titanium double oxide film on the surface of wood. On this basis, Zr⁴⁺ ions were introduced to further modify the photocatalytic performance and aging resistance of the wood surface and achieve improved self-cleaning.

EXPERIMENTAL

Materials

The wood samples consisted of *Eucalyptus* taken from Liangfengjiang National Forest Park (Nanning, Guangxi, China). After the wood specimens were air-dried to a water content of 15%, they were processed into specifications of 25 mm (L) × 25 mm (R) × 3 mm (T), washed in an ultrasonic bath for 15 min, and dried. The organic solvents and chemical reagents included butyl titanate (Damao Chemical Reagent Factory, Tianjin, China), tetraethyl orthosilicate (Kelon Chemical Reagent Factory, Chengdu, China), anhydrous ethanol (Damao Chemical Reagent Factory, Tianjin, China), nitric acid (Jinshan Chemical Reagent Co., Ltd, Chengdu, China), acetylacetone (Kelon Chemical Reagent Factory, Chengdu, China), zirconium oxychloride (Diyang Chemical Co., Ltd, Shanghai, China), and ultrapure water. Unless otherwise specified, they were not subjected to further treatment before use.

Methods

The tetraethyl orthosilicate, anhydrous ethanol, ultrapure water, and acetylacetone were mixed at a ratio of 1:6:8:0.05, respectively, and nitric acid was then added to adjust the pH to 2 to 3; the mixture was heated and stirred at room temperature for future use. The composite film made of pure silica gel was referred to as the silicon composite film (SCF). The tetrabutyl titanate, anhydrous ethanol, ultrapure water, acetylacetone, and nitric acid were mixed in two steps at a ratio of 1:10:2:0.5:0.2, respectively. The tetrabutyl titanate was first mixed with two-thirds of anhydrous ethanol and acetylacetone to form solution A. After vigorous stirring of solution A for 5 min, solution B was prepared by mixing one-third each of anhydrous ethanol, ultrapure water, and nitric acid. The mixed solution was stirred for 30 min. The composite film prepared from pure titanium was referred to as TCF. After the silicon-titanium sol was mixed, different mass fractions of zirconium oxychloride and zirconium oxychloride were added as zirconium ion precursor materials. The sol had different zirconium ion doping contents and was heated and stirred for 30 min and left until use. The doping amounts of zirconium oxychloride were 0.1 wt%, 0.5 wt%, 1 wt%, 2.5 wt%, 5 wt%, and 10 wt%, which were as denoted as STCF-0.1, STCF-0.5, STCF-2.5, STCF-5, and STCF-10, respectively. Other ratios of composite films were prepared to determine the properties. The prepared composite membrane samples are shown in Table 1. The prepared sol was aged for 3 h before filming.

After the configuration of the sol was complete, the dried wood pieces were removed and immersed in the sol for 3 h. After impregnation, the wood block was aged at room temperature for 12 h to form a uniform film on the surface of the wood. Then, it was placed in a drying oven at 103 °C for 6 h to complete the preparation of the composite film on the surface of the wood and obtain a Zr⁴⁺ doping SiO₂/TiO₂ film material on the surface of the wood.

The surface morphologies and elemental compositions of the samples were examined *via* an S-3400N scanning electron microscope (Hitachi, Ltd., Tokyo, Japan) and PV8200 energy dispersive energy spectrometry (Hitachi, Ltd., Tokyo, Japan). A gold foil (Au) layer was sputtered on the surface of the sample to improve conductivity before observation (GVC-1000; Hezao Electronic Technology Co., Ltd., Shanghai, China).

The XRD analyses used a Rigaku SmartLab X-ray diffractometer (Rigaku Corporation, Tokyo, Japan) with Cu K α ($\lambda = 1.5406 \text{ \AA}$) as the radiation source scanning at 2°/min with $2\theta = 15^\circ$ to 85° . The acceleration voltage and acceleration current were 40 kV

and 30 mA, respectively. The XRD data were compared with the JCPDS database to obtain the crystal phase.

Table 1. Composite Film Preparation Process

Acronym of Sample	Sample Content	Amount of Zr ⁴⁺ (Mass Ratio vs. Total Sample)	Silicon to Titanium Molar Ratio
SCF	SiO ₂	-	-
TCF	TiO ₂	-	-
STCF-0(STCF)	SiO ₂ /TiO ₂	-	1:3
STCF-0.1	Zr-SiO ₂ /TiO ₂	0.1%	1:3
STCF-0.5	Zr-SiO ₂ /TiO ₂	0.5%	1:3
STCF-1	Zr-SiO ₂ /TiO ₂	1.0%	1:3
STCF-2.5	Zr-SiO ₂ /TiO ₂	2.5%	1:3
STCF-5	Zr-SiO ₂ /TiO ₂	5.0%	1:3
STCF-10	Zr-SiO ₂ /TiO ₂	10%	1:3
1:1STCF-1	Zr-SiO ₂ /TiO ₂	1.0%	1:1
1:5STCF-1	Zr-SiO ₂ /TiO ₂	1.0%	1:5

The chemical structures of the groups in the composite films were analyzed *via* a Nicolet iS 50 Fourier transform infrared spectrophotometer (Thermo Fisher Scientific Corporation, Waltham, America). The scanning range of the instrument was 4000 cm⁻¹ to 400 cm⁻¹, and the resolution was 32 cm⁻¹. Pellets were used for FTIR analysis. The sample for FTIR characterization was prepared by scraping off the film from a wood substrate with a stainless-steel knife. The scraped sample powder was passed through a 100-mesh sieve, mixed with potassium bromide, and ground in a mortar to form a homogeneous mixture. The mixture was placed in a cylindrical mold (Tuopu Instrument Co., Ltd., Tianjin, China) with a diameter of 13 mm and pressed at 200 MPa for about 1 min to form a colorless transparent pellet.

The XPS test was performed on an Escalab 250Xi (Thermo Fisher Scientific Corporation, Waltham, America) Thermo instrument using a monochromatic Al target ($h\nu = 1486.6$ eV) as the X-ray source with a spot size of 500 μm . The full spectrum scan range was 0 eV to 1400 eV with narrow area scans of C1s, Si2p, Ti2p, and Zr3d. The calibration was performed by setting the binding energy of the indefinite carbon (C1s) to 284.8 eV. The data measured by XPS analysis were compared with the data in the *Handbook of X-ray Photoelectron Spectroscopy* (Perkin Elmer Ltd., Waltham, MA, USA) to determine the valence states and binding modes of the elements.

The parameters of the porous structure of the sample were measured by N₂ adsorption (ASAP 2460; Micromeritics Instruments Ltd., Atlanta, GA, USA). Before adsorption, the sample was vacuumed at 376 K in an evacuation chamber, and the specific surface area of the sample was calculated by the Brunauer-Emmett-Teller (BET) method, and the mesopores were obtained by the BJH method. The specific surface area, pore volume, and pore size distribution of the sample were tested with the DFT method.

The photocatalytic activity of the Zr⁴⁺-doped STCF was evaluated by its photodegradation ability on a methyl orange solution. The experimental variables were the Zr⁴⁺ doping level (0 wt%, 0.5 wt%, 1 wt%, and 2.5 wt%) and silicon to titanium molar ratio (1:1, 1:3, and 1:5). The photocatalytic reaction used a custom device. The samples were immersed in a beaker containing 100 mL of methyl orange (Jinshan Chemical Reagent Co., Ltd., Chengdu, China) solution (10 mg/L), and the initial pH of the methyl orange solution was 5. The ultraviolet irradiation source was 20 cm from the surface of the methyl orange

solution. Before irradiation, the reaction solution was kept in the dark and stirred for 30 min to establish the adsorption and desorption equilibrium between the samples to be tested and the methyl orange solution. During the photoreaction, the wood samples coated with the composite films were irradiated with a UV lamp (14 W, 365 nm) (Feiyang Instrument Co., Ltd., Jiangyin, China) under magnetic stirring, and the reaction was performed in air under room temperature. The concentration of the methyl orange supernatant was measured at different times (0.5 h, 1 h, 2 h, and 4 h). The absorbance value of methyl orange solution was characterized by the UV absorption intensity corresponding to the maximum absorption wavelength of methyl orange at 463 nm. Finally, the concentration of the residual methyl orange (η) was calculated after measuring the SP-75 visible spectrophotometer (Shanghai Spectrometer Co., Ltd., Shanghai, China) using Eq. 1,

$$\eta = C \div C_0 \times 100\% \quad (1)$$

where C_0 is the initial concentration (mg/L) of methyl orange aqueous solution, and C is the concentration (mg/L) of methyl orange solution after ultraviolet light irradiation.

The artificial aging of wood loaded with a ternary oxide film was carried out using an ultraviolet accelerated aging instrument (QUV/SPRAY; Wenkaier Trading Ltd., Foshan, China), and the aging resistance of wood was measured by the change in wood surface color. The lamp type was UVA-340, the light intensity was 0.89 W/m^2 , the temperature in the control experiment box was $60 \text{ }^\circ\text{C}$, and the condensation temperature was $50 \text{ }^\circ\text{C}$. The experiment was cycled with 8 h light, 15 min spray, and 3.45 h condensation. Using the International Standard Lighting Commission CIE1976 system, the surface chromaticity coordinates of each sample after photoaging for 0 h, 2 h, 4 h, 8 h, 12 h, 24 h, 48 h, 72 h, 96 h, and 120 h were measured using an ADCI-60-C automatic colorimeter (Chentaike Instrument Technology Ltd., Beijing, China). The values were L^* (lightness), a^* (red-green index), and b^* (yellow-blue index). Three samples were taken for each horizontal experiment, and three points were taken from the surface of each sample to obtain the average value of the measurements. The color difference was then calculated on the surface of the sample before and after aging with Eq. 2 (Fu *et al.* 2016),

$$\Delta E = (\Delta L^2 + \Delta a^2 + \Delta b^2)^{1/2} \quad (2)$$

where ΔL is the variation value of lightness, and Δa and Δb are the variation values of chroma.

RESULTS AND DISCUSSION

Surface Morphology

The morphologies of the silicon-titanium composite film and the Zr^{4+} -doped composite film are shown in Fig 1. Figures 1a and 1b show that the composite films before and after Zr^{4+} doping did not agglomerate, which indicates that the three precursors that participated in the reaction were uniformly dispersed. Compared with the undoped Zr^{4+} composite film (Fig. 1a), the doped 10 wt% zirconium composite film (Fig. 1b) had white nano-like convex substances that indicated that the silicon-titanium element in the composite film was present in the form of nanoparticles. A similar result has been described previously (Valdez-Castro *et al.* 2001). The surface of the undoped Zr^{4+} composite film was smooth and flat, and the structure was dense. The doped Zr^{4+} composite film appeared as white matter, and the nano-particle-like silicon-titanium ions were bound to the surface.

The white substance was likely an oxide formed by zirconium ions, and it was uniformly dispersed on the network structure composite film composed of SiO₂-TiO₂. The zirconium ions were slightly larger than titanium ions, and they are typical metal ions. Thus, it was difficult for the Zr to react with nonmetals. They were doped in an ionic state in the network structure of the SiO₂-TiO₂ oxide film. The joint surface (Fig. 1c) of the wood surface and the composite film shows that the composite film was only supported on the surface of the wood, and the thickness was approximately 100 nm to 120 nm. It was unable to penetrate the interior of the wood without destroying the original structure inside the wood.

The basic composition (d) of the nano-coating was further analyzed by energy dispersive x-ray analysis (EDAX). The peak of the unlabeled element in the figure was Au from the conductive layer, and the carbon and oxygen were from the native wood. After surface treatment, strong titanium and zirconium peaks appeared, which indicate that the surface of the composite film was mainly titanium and zirconium. The composite film base layer close to the wood surface was likely composed primarily of SiO₂ followed by a TiO₂ layer, and the outermost layer was composed of ZrO₂.

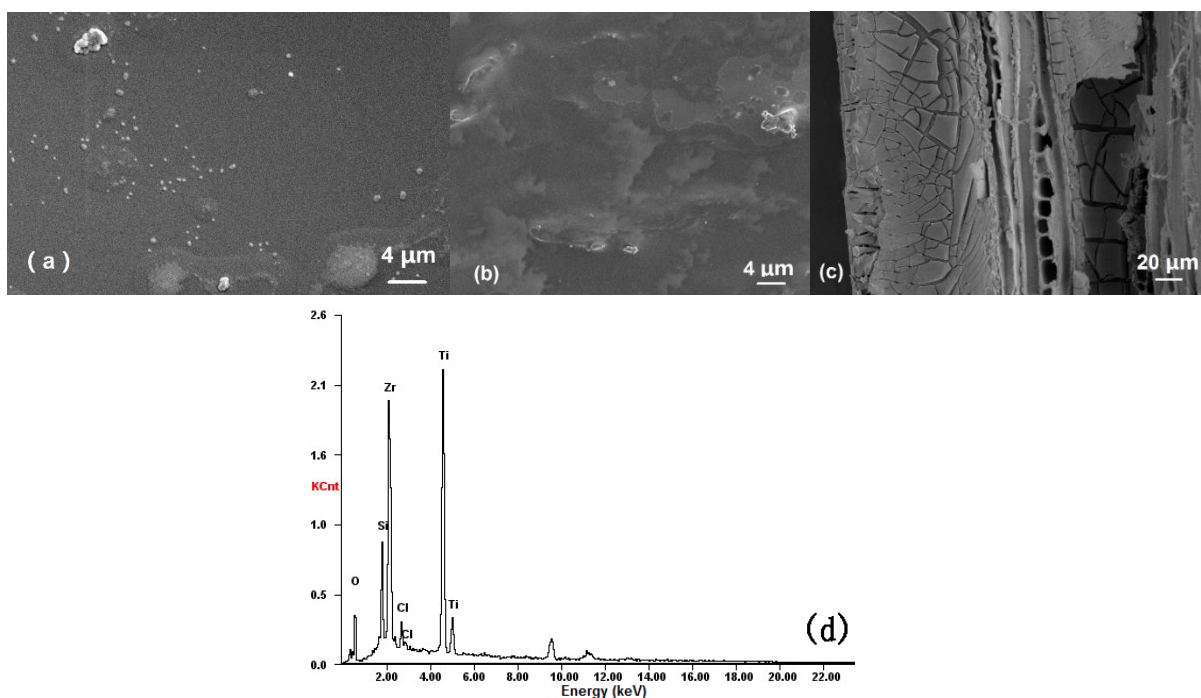


Fig. 1. SEM images of (a) STCF, (b) STCF doped with Zr⁴⁺, (c) the joint surface of the wood and composite film, and (d) the corresponding EDAX spectrum of STCF-1

Chemical Structure

The infrared spectrum of the STCF composite film obtained with different Zr⁴⁺ doping is shown in Fig. 2. The broad absorption band from 3600 cm⁻¹ to 3000 cm⁻¹ was mainly due to the combination of vibrations of uncondensed Si-OH, Ti-OH, and H₂O materials (Lenza and Vasconcelos 2001). The peaks at 2850 cm⁻¹ and 2958 cm⁻¹ were attributed to the CH stretching vibration of -CH₂ and -CH₃, respectively (Pandey 2015); the strong absorption peak that appeared at 1384 cm⁻¹ was attributed to the symmetric stretching vibration of nitrate NO₃⁻, *i.e.*, the reactant nitric acid was not completely involved in the reaction (Borca *et al.* 2008). The peaks at 1028 cm⁻¹ and 443 cm⁻¹

corresponded to the asymmetric stretching vibration of the Si-O-Si bond and the weak bending vibration of the Si-O-Si bond, respectively (Kongwudthiti *et al.* 2003). When doped with zirconium ions, the infrared spectra of the composite film showed a shoulder peak at 1632 cm^{-1} , which belonged to oxychloride bond. The absorption peak at 662 cm^{-1} was attributed to the Ti-O-Ti bond (Prabhakarrao *et al.* 2016), and the peak intensity was strengthened at 659 cm^{-1} mainly because of the presence of Zr-O-Zr bond. The absorption peak at 935 cm^{-1} was the vibration of the non-bridged oxygen Si-O bond in the Si-O tetrahedron, which is the Ti-O-Si characteristic peak (Zeitler and Brown 1957).

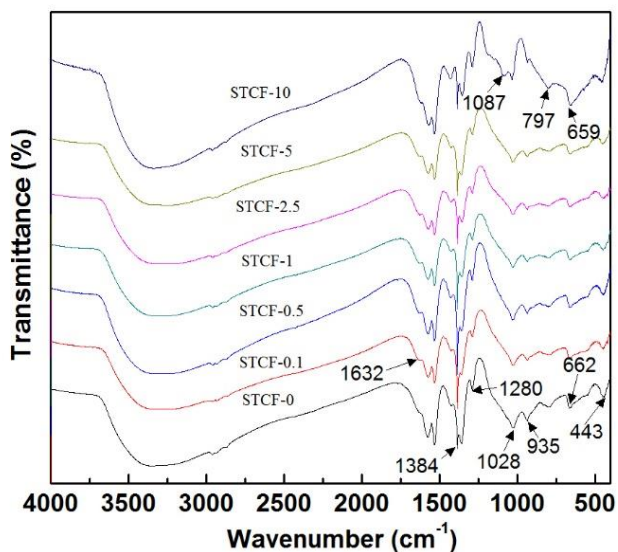


Fig. 2. FTIR spectra of STCF with different amounts of Zr^{4+} doping

Distribution of Elements

Figure 3 shows the narrow-area X-ray photoelectron peaks for C1s, Ti2p, Si2p, and Zr3d. The background was subtracted using Shirley's method (Ryo *et al.* 2016).

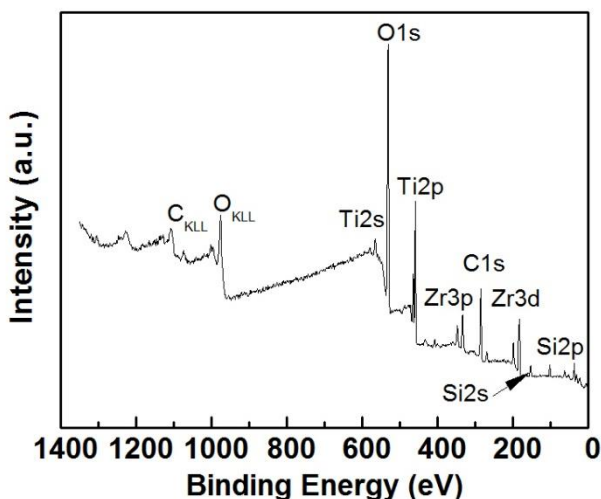


Fig. 3. Full XPS spectrum of STCF-1

Figure 4a shows the XPS spectrum of C1s in the composite film sample, which consisted of three peaks. The first peak was the -COOH compound bond, and the second peak was CO, *i.e.*, the alkoxy group that did not react completely during the reaction. The third peak was the CC peak (Jing *et al.* 2003). Figure 4b shows the Ti2p correlation spectral region of the measured composite membrane sample. The two spin-orbital components of the Ti2p peak (2p_{1/2} and 2p_{2/3}) had two curves (approximately 464.7 and 458.9, respectively). Good deconvolution indicated that the Ti ions in the composite film were all Ti⁴⁺ valence (Victor and Krupanidhi 2005). That is, the Ti⁴⁺ ions were all present in the form of TiO₂ and pure TiO₂ in the STCF composite film (2p_{1/2} = 464.2, 2p_{2/3} = 458.5).

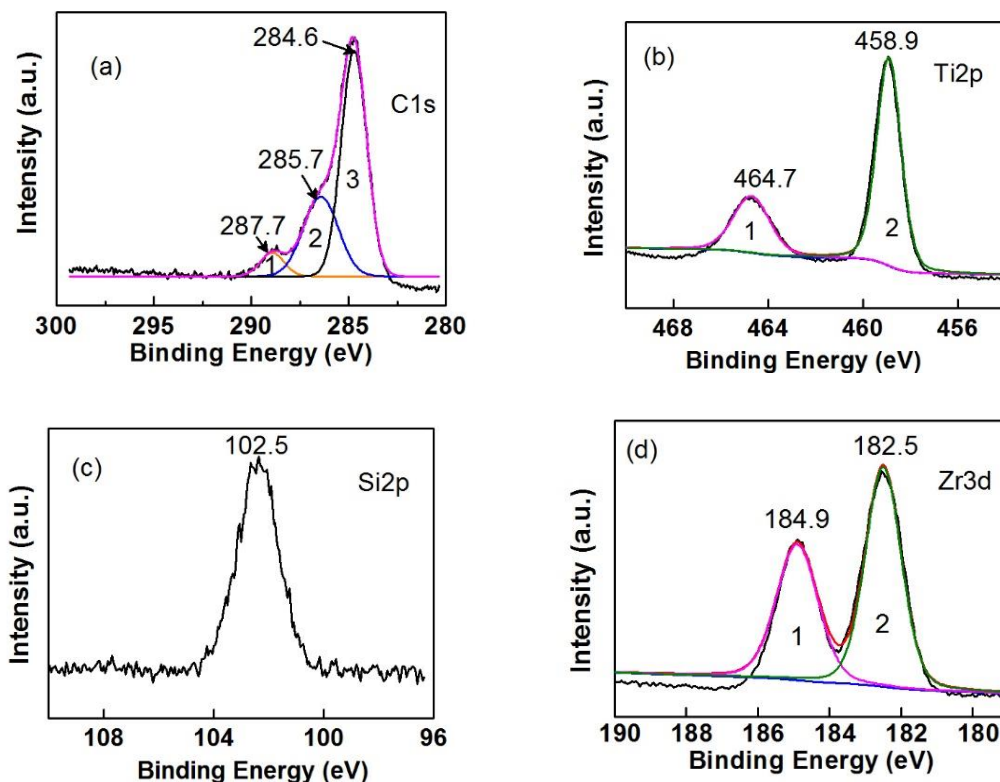


Fig. 4. XPS spectra of Zr⁴⁺-doped STCF: (a) C1s; (b) Ti2p; (c) Si2p; and (d) Zr3d

Compared with the increase in binding energy of the composite film, the results show that the Zr⁴⁺ ions were doped into the TiO₂ lattice (Huang *et al.* 2009). The Si2p peak XPS pattern of Fig. 3c indicates that Si ions were present in the Si⁴⁺ valence SiO₂ form in the composite film. Figure 3d shows the Zr3d spectral region in the XPS plot, in which two peaks were obtained by fitting analysis. The peak at 184.9 was Zr3d_{5/2}, and that at 182.5 was Zr3d_{3/2} for a difference of 2.4 eV. The reference manual confirms that zirconium ions were present in the form of ZrO₂ in the +4 valence state. As XPS Peaks41 software was used to obtain the peak area of all Zr and Ti peaks, the peak area was divided by the element sensitivity factor, and the mass ratio of Zr to Ti on the surface of the sample element was obtained. Samples with Zr/Ti ratio of 0.36 were prepared. The XPS data measured $x_2 = \text{Zr/Ti} = 0.34$, $x_2 < x$ because some zirconium ions could not enter the TiO₂ lattice and existed in the form of ZrO₂, which was similar to results reported in previous literature (Yu *et al.* 1998).

Crystal Structure

Figure 5 shows the XRD patterns of different Zr^{4+} ion-doped composite film samples. The literature states that the XRD diffraction peak of SiO_2 in the composite film component is an amorphous diffraction peak. The results show that the above composite films at different Zr^{4+} doping contained medium-intensity (101) diffraction peaks and weak-intensity (200) and (211) diffraction peaks, which are anatase phases of TiO_2 (JCPDS#21-1272). The activity of the anatase phase in TiO_2 is higher than that of the rutile phase (Zhang and Zeng 2010), which is advantageous for enhancing the photocatalytic performance. When the zirconium ion doping amount was 10 wt%, the diffraction peaks at (200) and (211) became very weak, and the diffraction peak intensity at (101) was reduced. The XRD pattern showed a slight shift to the bigger angle, but the Zr^{4+} -ion-related diffraction peaks (such as ZrO_2 and $ZrTiO_4$) have been not detected in the Zr^{4+} ion-doped composite film samples, indicating that the doping amount of zirconium ions had little effect on the crystal structure performance of the composite film.

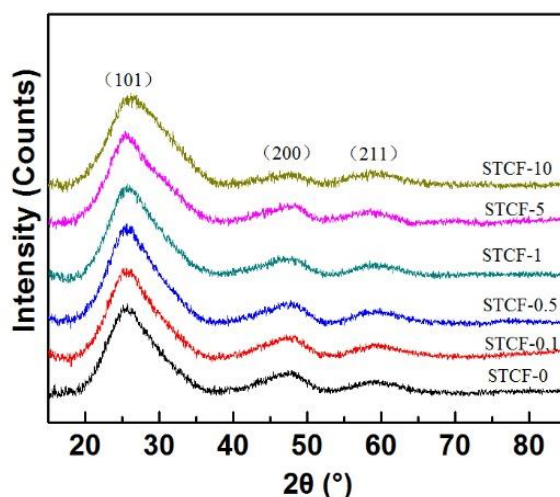


Fig. 5. XRD patterns of STCF with different Zr^{4+} doping

Analysis of the Pore Structure

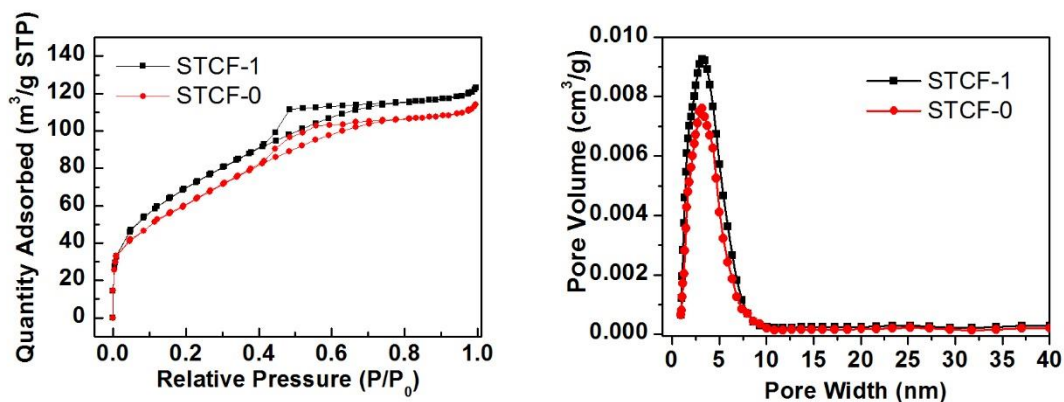


Fig. 6. (a) Adsorption and desorption isotherm of the STCF-0 and STCF-1 composite film; (b) Pore size distribution plots of the STCF-1 and STCF-0 composite film by the DFT method

The N₂ adsorption/desorption isotherm curves of STCF-1 and STCF-0 are shown in Fig. 6(a). From Fig 6(a), the adsorption isotherm of the samples are similar and belong to the combined isotherms of the second and fourth types, and the hysteresis loop appears here. The curve is slightly upturned when the relative pressure is close to 0.99, indicating that the material has a few micropores and some mesopores, which is consistent with the previous literature (Zhang and Li 2015). After doping Zr⁴⁺, the composite membrane samples exhibited a specific surface area and an average pore diameter of 259 m²/g and 2.94 nm, respectively. This is a higher specific surface area than the Zr_xTi_{1-x}O₂ catalyst prepared by Baojun Huang *et al.* (2013). The surface area determines the adsorption capacity of the material. A stronger adsorption capacity leads to a stronger degradation effect. The result is consistent with the degradation ability of the sample in the paper. Figure 6(b) shows pore size distribution (PSD) plots of STCF-1 and STCF-0 obtained by the DFT method. As can be seen in Fig. 6(b), the prepared samples have a narrow pore size distribution and the pore range is very similar for the two composite films, where pores mostly accumulated from 0.92 to 10.06 nm. It is also clear that, when the film is doped with Zr⁴⁺, the pore distribution widened and the pore volume increased correspondingly. This indicates that appropriate amount of Zr⁴⁺ doping could improve the pore structure of composite film (Shen *et al.* 2016).

Analysis on the Photocatalytic Activity

The effect of the composite membrane on the degradation of methyl orange contaminants is shown in Fig. 7. The initial time in the figure was a result of the absorbance measured after 3 h in the dark. The dark reaction reduced the variation of the in-composite membrane adsorption of methyl orange, which can decrease the absorbance of methyl orange. The unloaded composite film wood adsorbed methyl orange by 30% in the dark. After that, the degradation rate of methyl orange did not improve further with additional UV irradiation. This was because the substrate was saturated with methyl orange by 3 h in the dark. The wood itself could not degrade methyl orange contaminants and had no more surface area to adsorb methyl orange.

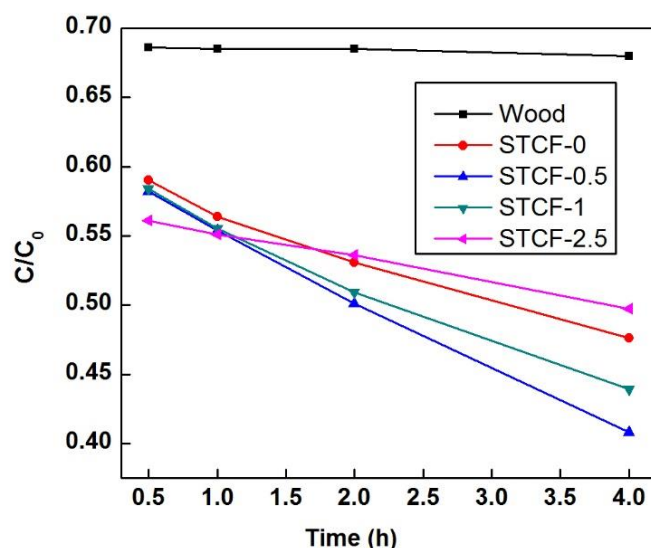


Fig. 7. Effect of Zr⁴⁺ doping on the degradation of methyl orange by STCF

At the end of the dark reaction stage, the ability of wood samples loaded with composite membrane to degrade methyl orange pollutants was noticeably improved compared to pure wood. Following the dark reaction stage, Zr^{4+} doping had no impact on the photocatalytic degradation of the composite membrane. This ability was mainly determined by the anatase crystalline TiO_2 in the composite film. In the early light stage (within the first 0.5 h), the degradation ability of all composite membranes to methyl orange pollutants was maximized. At that time, the composite membrane had the highest degradation ability to methyl orange at 2.5 wt% Zr^{4+} . The band gap energy of TiO_2 broadened because a large amount of Zr^{4+} quickly participated in the reaction, and the degradation rate rapidly increased. When the reaction time was gradually extended, the degradation ability of the STCF-2.5 composite film was lower than that of the undoped Zr^{4+} ions. The degradation ability of the composite membrane was likely due to the accumulation of a large amount of Zr^{4+} ions on the surface of the composite membrane. This hindered contact between the methyl orange and the composite membrane. The photocatalytic degradation ability mainly came from the composite membrane formed by TiO_2 and SiO_2 . The Zr^{4+} ions only served to increase the activity of the TiO_2 composite membrane. The degradation ability of pollutants in the late stage of the reaction gradually increased. In the selected experimental variables, the degradation ability of the composite membrane reached a maximum value when the Zr^{4+} doping amount was 0.5 wt%, but the degradation rate of all composite membranes decreased notably.

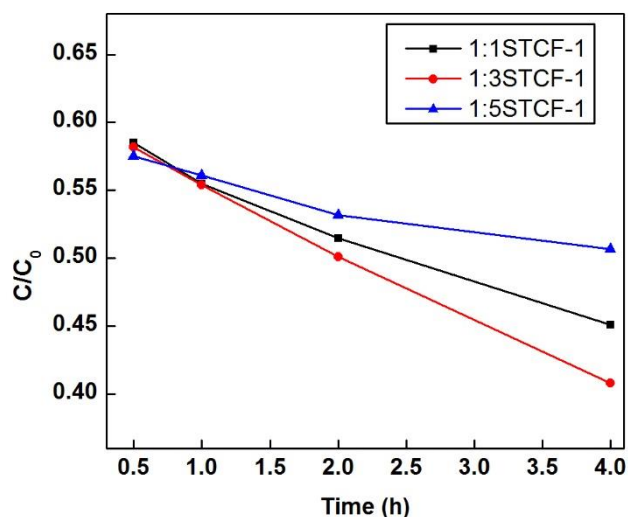


Fig. 8. Effect of Si/Ti ratios on the degradation of methyl orange by STCF

Figure.8 shows the photocatalytic degradation ability of STCF composite films with different Si/Ti ratios with the same Zr^{4+} ion doping amount (1 wt%). After the completion of the dark reaction stage, the photocatalytic degradation ability of the composite film with a silicon-titanium ratio of 1:5 was the strongest. At longer catalytic degradation times, the photocatalytic degradation ability of silicon-titanium was the highest with a silicon-titanium ratio of 1:3. The photocatalytic ability of the early stage likely relies mainly on the anatase crystalline TiO_2 to play a leading role. At longer times, the excessively high Ti^{4+} hindered the contact of the methyl orange contaminant with the composite membrane, thereby reducing the photocatalytic activity.

Analysis on Aging Resistance

The results show the effect of different Zr^{4+} ion doping amounts on the color change in ultraviolet light irradiation. The effects of ΔE and ΔL are shown in Figs. 9 and 10. The amount of Zr^{4+} ion doping had an obvious influence on the aging resistance of the composite film.

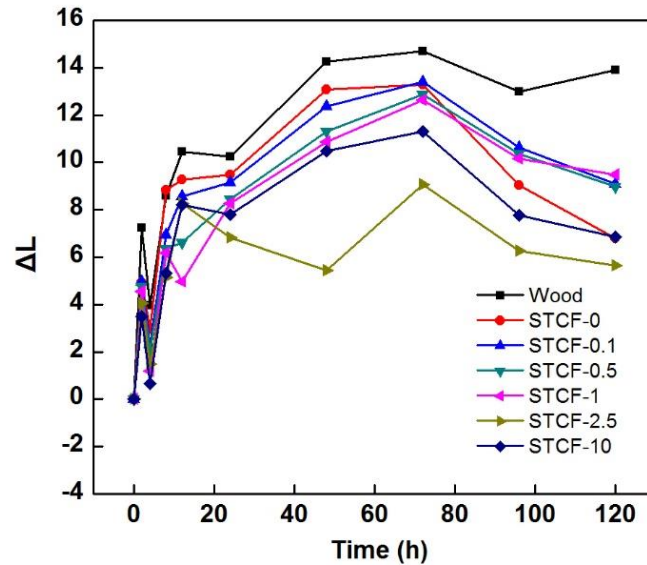


Fig. 9. ΔL variation of different Zr^{4+} ion doping STCF composite films during photoaging

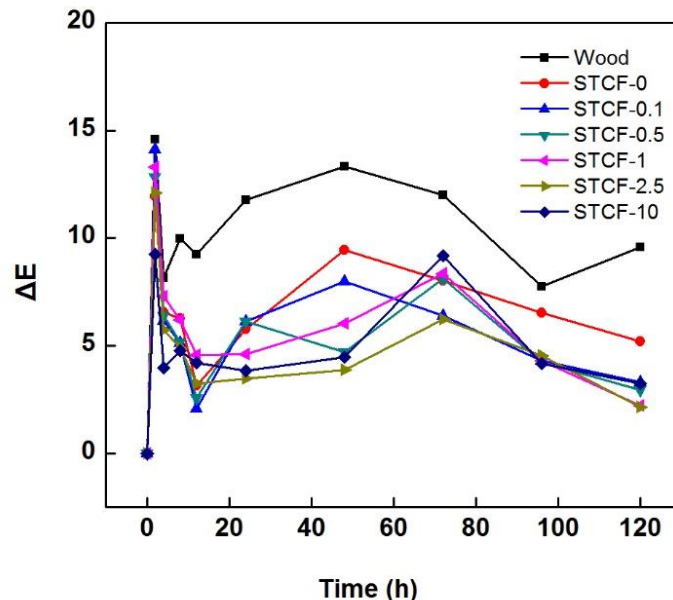


Fig. 10. ΔE variation of different Zr^{4+} ion doping STCF composite films during photoaging

The ΔL values for all composite membranes were positive, which indicates that the lightness increased, and the surface color began to fade after UV irradiation. The lightness of the wood sample loaded with the composite film decreased relative to the unloaded composite film wood. However, the degree of decline was lower than that of the former,

which indicates that fading under ultraviolet light irradiation was suppressed *via* the composite film. The degree of fading increased the aging resistance of wood, and fading decreased with increasing Zr⁴⁺ doping. At 2.5 wt%, the wood lightness index (L^*) remained the highest after 120 h of photoaging. The degree of minimization indicates that aging resistance was best under these conditions. Further, doping had no effect. The color change of the wood surface before and after UV treatment was represented by ΔE . The sample loaded with the composite film had a slightly smaller color change than the pure wood, and the wood color was relatively stable.

CONCLUSIONS

1. A Zr⁴⁺-doped silicon-titanium composite film was prepared on the surface of wood *via* a sol-gel method to improve the photocatalytic and photoaging resistance of the wood surface and achieve self-cleaning abilities.
2. The structural analysis of the composite membrane showed that a new Si-O-Ti bond was formed, which indicates that the networked silica was crosslinked with titanium dioxide, and the Si-O-Si absorption peak had a certain degree of displacement. This displacement likely generated Si-O-Si. The Zr bond interacted with Si-O-Si, and the composite film only showed the crystalline structure of TiO₂ with anatase crystal form.
3. There was a small movement at the (101) diffraction peak, confirming Zr⁴⁺ doping. The silicon, titanium, and zirconium in the composite film were present in the form of silica titania, and the Zr⁴⁺ existed in the form of ZrO₂, which was partially doped in an ionic state. The composite film sample contained a few mesopores, which promote the photocatalytic degradation of the wood surface.
4. After Zr⁴⁺ doping, the photoaging resistance and photocatalytic performance of the composite film samples increased notably. The photocatalytic ability of the methyl orange solution reached a maximum of 40.8% when the zirconium ion doping amount was 0.5 wt%. The resistance to ultraviolet aging was optimal when the zirconium ion doping amount was 2.5 wt%.

ACKNOWLEDGMENTS

The authors gratefully acknowledge financial support from the Guangxi Science and Technology Major Project (AA17204087-14) and the Special Fund of the National Natural Science Foundation of China (31560191).

REFERENCES CITED

- Aloui, F., Ahajji, A., Irmouli, Y., George, B., Charrier, B., and Merlin, A. (2007). "Inorganic UV absorbers for the photostabilisation of wood-clearcoating systems: Comparison with organic UV absorbers," *Appl. Surf. Sci.* 253(8), 3737-3745. DOI: 10.1016/j.apsusc.2006.08.029

- Borca, E., Bercu, M., Georgescu, S., Hodoroagea, S., and Cotoi, E. (2008). "XRD and FTIR characterization of nanocrystalline YVO₄: Eu derived by coprecipitation process," *Z. Kristallogr. Suppl.* 27, 121-126. DOI: 10.1524/zksu.2008.0016
- Chen, W., Zhou, X., Zhang, X., Feizbakhshan, M., Cao, Y., Shi, S., Nguyen, T., and Chen, M. (2018). "Fast formation of hydrophobic coating on wood surface *via* an energy-saving dielectric barrier discharges plasma," *Prog. Org. Coat.* 125, 128-136. DOI: 10.1016/j.porgcoat.2018.06.018
- Fu, Y., Liu, X., Cheng, F., Sun, J., and Qin, Z. (2016). "Modification of the wood surface properties of *Tsoongiodendron odorum* Chun with silicon dioxide by a sol-gel method," *BioResources* 11(4), 10273-10285. DOI: 10.15376/biores.11.4.10273-10285
- Guo, H., Büchel, M., Li, X., Wäckerlin, A., Chen, Q., and Burgert, I. (2018). "Dictating anisotropic electric conductivity of a transparent copper nanowire coating by the surface structure of wood," *J. R. Soc. Interface.* 15, Article ID 20170864. DOI: 10.1098/rsif.2017.0864
- Huang, B., Liu, M., Zhang, Y., Li, P., and Zheng, Z. (2013). "Synthesis of Zr-doped TiO₂ templated from cloth and its photocatalytic activity," *Ionics* 19(4), 681-687. DOI: 10.1007/s11581-012-0785-x
- Huang, Y., Ho, W., Ai, Z., Song, X., and Lee, S. (2009). "Aerosol-assisted flow synthesis of B-doped, Ni-doped and B-Ni-codoped TiO₂ solid and hollow microspheres for photocatalytic removal of NO," *Appl. Catal. B-Environ.* 89(3-4), 398-405. DOI: 10.1016/j.apcatb.2008.12.020
- Hubert, T., Unger, B., and Bucker, M. (2010). "Sol-gel derived TiO₂ wood compo-sites," *J. Sol-Gel Sci. Techn.* 53(2), 384-389. DOI: 10.1007/s10971-009-2107-y
- Kongwudthiti, S., Praserttham, P., Tanakulrungsank, W., and Inoue, M. (2003). "The influence of Si-O-Zr bonds on the crystal-growth inhibition of zirconia prepared by the glycothermal method," *J. Mater. Process. Tech.* 136(1), 186-189. DOI: 10.1016/S0924-0136(03)00157-2
- Korkut, D. S., Korkut, S., Bekar, I., Budakçı, M., Dilik, T., and Çakıcıer, N. (2008). "The effects of heat treatment on the physical properties and surface roughness of Turkish hazel (*Corylus colurna* L.) wood," *Int. J. Mol. Sci.* 9(9), 1772-1783. DOI: 10.3390/ijms9091772
- Lenza, R. F. S., and Vasconcelos, W. L. (2001). "Preparation of silica by sol-gel method using formamide," *J. Mater. Res.* 4(3), 189-194. DOI: 10.1590/S1516-14392001000300008
- Jing, L., Sun, X., Cai, W., Xu Z., Du, Y., and Fu, H. (2003). "The preparation and characterization of nanoparticle TiO₂/Ti films and their photocatalytic activity," *J. Phys. Chem. Solids* 64(4), 615-623. DOI: 10.1016/s0022-3697(02)00362-1
- Mahendran, A. R., Wuzella, G., Aust, N., Kandelbauer, A., and Müller, U. (2011). "Photocrosslinkable modified vegetable oil based resin for wood surface coating application," *Prog. Org. Coat.* 74(4), 697-704. DOI: 10.1016/j.porgcoat.2011.09.027
- Mahlting, B., Arnold, M., and Löthman, P. (2010). "Surface properties of sol-gel treated thermally modified wood," *J. Sol-Gel Sci. Techn.* 55(2), 221-227. DOI: 10.1007/s10971-010-2236-3
- Mahr, M. S., Hübert, T., Stephan, I., Bucker, M., and Militz, H. (2013). "Reducing copper leaching from treated wood by sol-gel derived TiO₂ and SiO₂ depositions," *Holzforschung.* 67(4), 429-435. DOI: 10.1515/hf-2012-0105

- Muff, L. F., Luxbacher, T., Burgert, I., and Michen, B. (2018). "Investigating the time-dependent zeta potential of wood surfaces," *J. Colloid Interf. Sci.* 518, 165-173. DOI: 10.1016/j.jcis.2018.02.022
- Pandey, K. K. (2015). "A study of chemical structure of soft and hardwood and wood polymers by FTIR spectroscopy," *J. Appl. Polym. Sci.* 71(12), 1969-1975. DOI: 10.1002/(SICI)1097-4628(19990321)71:12<1969::AID-APP6>3.0.CO;2-D
- Prabhakar Rao, N., Chandra, M. R., and Rao, T. S. (2016). "Synthesis of Zr doped TiO₂ /reduced graphene oxide (rGO) nanocomposite material for efficient photocatalytic degradation of dyes under visible light irradiation," *J. Alloy. Compd.* 694, 596-606. DOI: 10.1016/j.jallcom.2016.09.329
- Qian, T., Dang, B., Chen, Y., Jin, C., Qian, J., and Sun, Q. (2019). "Fabrication of magnetic phase change n-eicosane @Fe₃O₄/SiO₂ microcapsules on wood surface via sol-gel method," *J. Alloy. Compd.* 772, 871-876. DOI: 10.1016/j.jallcom.2018.09.125
- Rosu, D., Teaca, C. A., and Bodirlau, R. (2010). "FTIR and color change of the modified wood as a result of artificial light irradiation," *J. Photoch. Photobio. B* 99(3), 144-149. DOI: 10.1016/j.jphotobiol.2010.03.010
- Ryo, M., Yugo N., Noriyuki K., Hiromi T., Hideki Y., Shigeo T., and Kazuhiro Y. (2016). "Reproducibility of XPS analysis for film thickness of SiO₂/Si by active Shirley method," *J. Electron Spectrosc. Relat. Phenom.* 207:55-59. DOI: 10.1016/j.elspec.2015.12.008
- Shen, Z., Zhong, J., Wang, L., Zheng, Y., Cui, Y., and Chen, L. (2016). "In-situ FTIR and SSNMR study of photocatalytic degradation of 2-CEES and DMMP on zirconium-doped TiO₂" *J. Mol. Catal.* 30(3), 260-268. DOI: 10.16084/j.cnki.issn1001-3555.2016.03.006
- Valdez-Castro, L., Méndez-Vivar, J., and Mendoza-Serna, R. (2001). "Porous SiO₂-TiO₂-ZrO₂ obtained from polymeric systems prepared by the sol-gel process," *J. Porous Mat.* 8(4), 303-309. DOI: 10.1023/A:1013117131821
- Victor, P., and Krupanidhi, S. B. (2005). "Impact of microstructure on electrical characteristics of laser ablation grown ZrTiO₄ thin films on Si substrate," *J. Phys. D. Appl. Phys.* 38(1), 41. DOI: 10.1088/0022-3727/38/1/009
- Wang, B., Feng, M., and Zhang H. (2013). "Research progress on surface functional modification of wood," *China Surface Engineering* 26(6), 9-17. DOI: 10.3969/j.issn.1007-9289.2013.06.002
- Wright, N. C., Li, J., and Guo, M. (2006). "Microstructural and mold resistant properties of environment-friendly oil-modified polyurethane based wood-finish products containing polymerized whey proteins," *J. Appl. Polym. Sci.* 100(5), 3519-3530. DOI: 10.1002/app.22432
- Xuan, L., Fu, Y., Liu, Z., Wei, P., and Wu, L. (2018). "Hydrophobicity and photocatalytic activity of a wood surface coated with a Fe³⁺-doped SiO₂/TiO₂ film," *Materials* 11(12), 2594-2609. DOI: 10.3390/ma11122594
- Yuan, B., Ji, X., Thang, N. T., Huang, Z., and Guo, M. (2018). "UV protection of wood surfaces by graphitic carbon nitride nanosheets," *Appl. Surf. Sci.* 467-468, 1070-1075. DOI: 10.1016/j.apsusc.2018.10.251
- Yu, J. C., Lin, J., and Kwok, R. W. M. (1998). "Ti_{1-x}Zr_xO₂ solid solutions for the photocatalytic degradation of acetone in air," *J. Phys. Chem. B* 102(26), 5094-5098. DOI: 10.1021/jp980332e

- Zeitler, V. A., and Brown, C. A. (1957). "The infrared spectra of some Ti-O-Si, Ti-O-Ti and Si-O-Si compounds," *J. Phys. Chem.* 61(9), 1174-1177. DOI: 10.1021/j150555a010
- Zhang, D., and Zeng, F. (2010). "Structural, photochemical and photocatalytic properties of zirconium oxide doped TiO₂ nanocrystallites," *Appl. Surf. Sci.* 257(3), 867-871. DOI: 10.1016/j.apsusc.2010.07.083
- Zhang, Y., and Li, P. (2015). "Photocatalytic membranes prepared by embedding porous Zr-doped SiO₂ shell/TiO₂ core particles with expanded channels into polyvinylidene fluoride for cleaning wastewater," *RSC Adv.* 5, 98118-98129. DOI: 10.1039/c5ra16319f

Article submitted: March 27, 2020; Peer review completed: May 16, 2020; Revised version received and accepted: June 28, 2020; Published: July 2, 2020.
DOI: 10.15376/biores.15.3.6404-6419